

## Interfacial spin-orbit torque without bulk spin-orbit coupling

Satoru Emori,<sup>\*</sup> Tianxiang Nan,<sup>†</sup> Amine M. Belkessam, Xinjun Wang, Alexei D. Matyushov, Christopher J. Babroski, Yuan Gao, Hwaider Lin, and Nian X. Sun

*Department of Electrical and Computer Engineering, Northeastern University, Boston, Massachusetts 02115, USA*

(Received 28 January 2016; revised manuscript received 12 April 2016; published 4 May 2016)

An electric current in the presence of spin-orbit coupling can generate a spin accumulation that exerts torques on a nearby magnetization. We demonstrate that, even in the absence of materials with strong bulk spin-orbit coupling, a torque can arise solely due to interfacial spin-orbit coupling, namely, Rashba-Edelstein effects at metal/insulator interfaces. In magnetically soft NiFe sandwiched between a weak spin-orbit metal (Ti) and insulator ( $\text{Al}_2\text{O}_3$ ), this torque appears as an effective field, which is significantly larger than the Oersted field and qualitatively modified by inserting an additional layer between NiFe and  $\text{Al}_2\text{O}_3$ . Our findings point to unconventional routes for tuning spin-orbit torques by engineering interfacial electric dipoles.

DOI: [10.1103/PhysRevB.93.180402](https://doi.org/10.1103/PhysRevB.93.180402)

An electric current in a thin film with spin-orbit coupling can produce a spin accumulation [1–3] which can then exert sizable torques on magnetic moments [4–7]. First demonstrated in a ferromagnetic semiconductor [8], “spin-orbit torques” are nowadays studied in room-temperature ferromagnetic metals (FMs) interfaced with heavy metals (HMs) with strong spin-orbit coupling, such as Pt, Ta, and W [9–25]. These torques can arise from (1) spin-dependent scattering of conduction electrons in the bulk of the HM, i.e., the spin Hall effect [2,3,9–13], and (2) momentum-dependent spin polarization at the HM/FM interface, i.e., the Rashba-Edelstein effect [1,5,14–17]. Since a HM/FM system can exhibit either or both of these spin-orbit effects, it can be a challenge to distinguish the spin Hall and Rashba-Edelstein contributions [3,6,7,18,19]. Spin-orbit torques may be further influenced by spin scattering [26,27] or proximity-induced magnetization [28] at the HM/FM interface. Moreover, in many cases [9–25], the FM interfaced on one side with a HM is interfaced on the other with an insulating material, and the electric dipole at the FM/insulator interface [29,30] may also give rise to a Rashba-Edelstein effect. Recent studies [21–25] indeed suggest nontrivial influences from insulating oxide capping layers in perpendicularly magnetized HM/FM systems. However, with the FM only  $\lesssim 1$  nm thick [21–25], changing the degree of oxidation of the capping layer may modify the composition of the adjacent ultrathin FM and hence the HM/FM interface. The points above make it difficult to disentangle the contributions from the HM bulk, HM/FM interface, and FM/insulator interface, thereby posing a challenge for coherent engineering of spin-orbit torques.

Here, we experimentally show a spin-orbit torque that emerges exclusively from metal/insulator interfaces in the absence of materials with strong bulk spin-orbit coupling. Our samples consist of magnetically soft  $\text{Ni}_{80}\text{Fe}_{20}$  (NiFe) sandwiched between a weak spin-orbit light metal (Ti) and a weak spin-orbit insulator ( $\text{Al}_2\text{O}_3$ ). We observe a “fieldlike” spin-orbit torque that appears as a current-induced effective

field, which is significantly larger than the Oersted field. This torque is conclusively attributed to the Rashba-Edelstein effect, i.e., spin accumulation at the NiFe/ $\text{Al}_2\text{O}_3$  interface exchange coupling to the magnetization in NiFe [4,5]. Furthermore, an insertion layer at the NiFe/ $\text{Al}_2\text{O}_3$  interface qualitatively modifies this observed torque: Inserting an atomically thin layer of a strong spin-orbit metal (Pt) causes the fieldlike torque to vanish, whereas inserting a conductive weak spin-orbit metal (Cu) layer results in a “nonlocal” fieldlike torque where the spin accumulation couples to the magnetization in NiFe across Cu. Our findings demonstrate model systems exhibiting purely interfacial spin-orbit torques, which are free from complications caused by strong spin-orbit HMs, and open possibilities for spin-orbit torques enabled by engineered electric dipoles at interfaces.

Thin-film heterostructures are sputter deposited on Si substrates with a 50-nm-thick  $\text{SiO}_2$  overlayer. All layers are deposited at an Ar pressure of  $3 \times 10^{-3}$  Torr with a background pressure of  $\lesssim 2 \times 10^{-7}$  Torr. Metallic layers are deposited by dc magnetron sputtering, whereas  $\text{Al}_2\text{O}_3$  is deposited by rf magnetron sputtering from a stoichiometric target. The deposition rates are calibrated by x-ray reflectivity. For each structure, unless otherwise noted, a 1.2-nm-thick Ti seed layer is used to promote the growth of NiFe with a narrower resonance linewidth and near-bulk saturation magnetization. Devices are patterned and contacted by Cr(3 nm)/Au(100 nm) electrodes by photolithography and liftoff.

We first examine the current-induced field in a trilayer of Ti(1.2 nm)/NiFe(2.5 nm)/ $\text{Al}_2\text{O}_3$ (1.5 nm) by using the second-order planar Hall effect (PHE) voltage technique devised by Fan *et al.* [10,11]. As illustrated in Fig. 1(a), a dc current  $I_{dc}$  along the  $x$  axis generates a planar Hall voltage  $V_{PH}$  along the  $y$  axis in a 100- $\mu\text{m}$ -wide Hall bar, which is placed in the center of a two-axis Helmholtz coil. The second-order planar Hall voltage  $\Delta V_{PH} = V_{PH}(+I_{dc}) + V_{PH}(-I_{dc})$  is measured while sweeping the external field  $H_x$  [Fig. 1(b)]. The total current-induced in-plane transverse field  $H_I$  (which includes the Oersted field) pulls the magnetization away from the  $x$  axis at an angle  $\theta$ . When  $|H_x|$  is large enough ( $\gtrsim 10$  Oe) to magnetize the soft NiFe layer nearly uniformly,  $\theta$  is small and  $\Delta V_{PH}$  is proportional to  $I_{dc}^2 H_x^{-1} dH_I/dI_{dc}$  [10]. Following the procedure in Ref. [11] (with data at  $|H_x| < 10$  Oe discarded to eliminate spurious effects from nonuniform

<sup>\*</sup>Present address: Geballe Laboratory for Advanced Materials, Stanford University, Stanford, CA 94305, USA; satorue@stanford.edu

<sup>†</sup>Present address: Department of Materials Science and Engineering, University of Wisconsin Madison, Madison, WI 53706, USA.

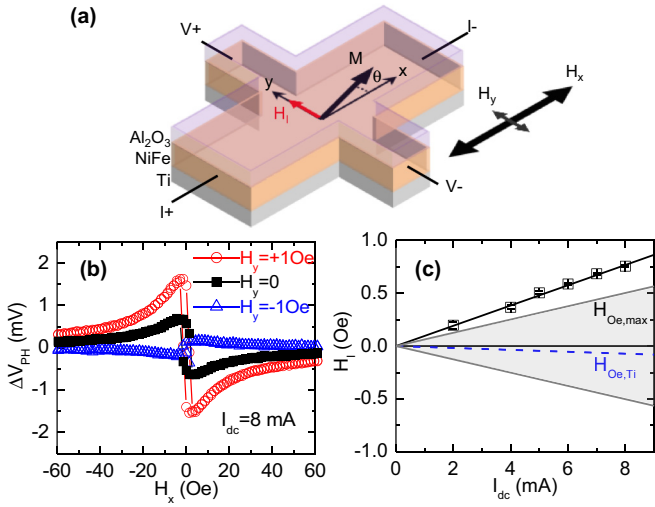


FIG. 1. (a) Schematic of the second-order PHE measurement. (b) Second-order planar Hall voltage  $\Delta V_{\text{PH}}$  curves at different transverse bias fields  $H_y$ . (c) Current-induced field  $H_I$  vs  $I_{\text{dc}}$ . The dotted line shows  $H_{\text{Oe,Ti}}$  based on the estimated fraction of  $I_{\text{dc}}$  in Ti. The shaded area is bounded by the maximum possible Oersted field  $H_{\text{Oe,max}}$ .

magnetization), we apply a constant transverse bias field  $|H_y| = 1$  Oe [Figs. 1(a) and 1(b)] and extrapolate the critical  $H_y$  required to cancel  $H_I$ , i.e., to null the  $\Delta V_{\text{PH}}$  spectrum. For the data in Fig. 1(b),  $H_y = -0.75$  Oe would null  $\Delta V_{\text{PH}}$ , so  $H_I = 0.75$  Oe at  $I_{\text{dc}} = 8$  mA.

As shown in Fig. 1(c),  $H_I$  scales linearly with  $I_{\text{dc}}$  with slope  $dH_I/dI_{\text{dc}} = 0.095$  Oe per mA. To estimate the Oersted field contribution to  $H_I$ , the current is assumed to be uniform within each conductive layer, such that the Oersted field comes only from the current in the Ti layer,  $H_{\text{Oe,Ti}} = f_{\text{Ti}} I_{\text{dc}}/2w$ , where  $f_{\text{Ti}}$  is the fraction of  $I_{\text{dc}}$  in Ti and  $w$  is the Hall bar width. The sheet resistances of  $2000 \Omega/\text{sq}$  for Ti (1.2 nm) and  $350 \Omega/\text{sq}$  for NiFe (2.5 nm), found from four-point resistance measurements on a series of films (each with an insulating capping layer that prevents oxidation), yield  $f_{\text{Ti}} = 0.15$  and  $|H_{\text{Oe,Ti}}| = 0.009$  Oe per mA. The net  $H_I$  is therefore an order of magnitude larger than  $H_{\text{Oe,Ti}}$ , and, moreover, the direction of  $H_I$  opposes  $H_{\text{Oe,Ti}}$ .

The actual Oersted field may deviate from  $H_{\text{Oe,Ti}}$  because of a nonuniform current distribution within each conductive layer and interfacial scattering, both of which are difficult to quantify. However, we can place the upper bound on the Oersted field,  $|H_{\text{Oe,max}}| = |I_{\text{dc}}|/2w$ , by assuming that the *entire*  $I_{\text{dc}}$  flows above or below the magnetic layer. In Fig. 1(c), we shade the range bounded by  $|H_{\text{Oe,max}}|$ . The magnitude of  $H_I$  still exceeds  $H_{\text{Oe,max}}$ , confirming the presence of an additional current-induced field with a component collinear with the Oersted field.

We also measure  $H_I$  with a technique based on spin-torque ferromagnetic resonance (ST-FMR) [31,32]. As illustrated in Fig. 2(a), the rf excitation current is injected into a  $5\text{-}\mu\text{m}$ -wide,  $25\text{-}\mu\text{m}$ -long strip through a ground-signal-ground electrode. While the in-plane external field  $H$  is swept at an angle  $\theta$ , the rectified mixing voltage  $V_{\text{mix}}$  across the strip is acquired with a lock-in amplifier [33]. The resulting spectrum [e.g., Fig. 2(b)] is well fit to a Lorentzian curve

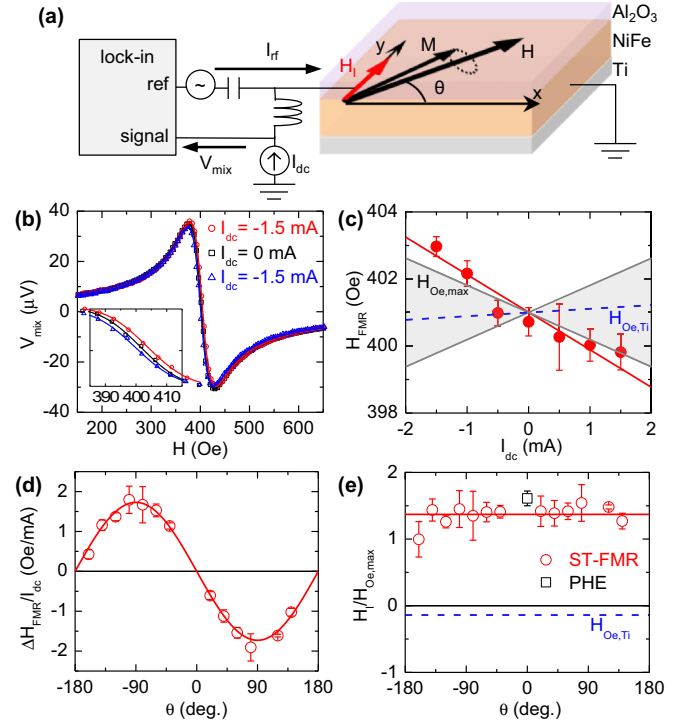


FIG. 2. (a) Schematic of the ST-FMR setup. (b) ST-FMR spectra at different dc bias currents  $I_{\text{dc}}$ , with rf current excitation at 5 GHz and +8 dBm and external field  $H$  at  $\theta = 40^\circ$ . Inset:  $I_{\text{dc}}$ -induced shift of ST-FMR spectra. (c) Shift of resonance field  $H_{\text{FMR}}$  due to  $I_{\text{dc}}$  at  $\theta = 40^\circ$ . The error bar is the standard deviation of five measurements. The dotted line shows the estimated Oersted field from Ti,  $H_{\text{Oe,Ti}}$ . The shaded area is bounded by the maximum possible Oersted field,  $H_{\text{Oe,max}}$ . (d) Angular dependence of  $I_{\text{dc}}$ -induced  $H_{\text{FMR}}$  shift. The error bar is the error in linear fit of  $H_{\text{FMR}}$  vs  $I_{\text{dc}}$ . The solid curve indicates the fit to  $\sin \theta$ . (e) Transverse current-induced field  $H_I = -\Delta H_{\text{FMR}}/\sin \theta$  normalized by  $H_{\text{Oe,max}}$  at various  $\theta$ . The solid line indicates the average of the ST-FMR data points. The dotted line indicates estimated  $H_{\text{Oe,Ti}}$ . The PHE data point at  $\theta = 0$  is the average of three devices.

$V_{\text{mix}} = V_s F_s + V_a F_a$  consisting of the symmetric component  $F_s = W^2/[(H - H_{\text{FMR}})^2 + W^2]$  and antisymmetric component  $F_a = W(H - H_{\text{FMR}})/[(H - H_{\text{FMR}})^2 + W^2]$ , where  $W$  is the resonance linewidth and  $H_{\text{FMR}}$  is the resonance field. We inject a small dc bias current  $|I_{\text{dc}}| \leq 2$  mA to measure the shift in  $H_{\text{FMR}}$  caused by the net  $I_{\text{dc}}$ -induced field  $H_I$  [33]. Although the scatter in the ST-FMR data is greater than the PHE data [Fig. 1(c)], Fig. 2(c) shows that the observed shift in  $H_{\text{FMR}}$  is significantly larger than (and opposes) the contribution from  $H_{\text{Oe,Ti}}$ , and its magnitude exceeds the maximum possible shift from  $H_{\text{Oe,max}}$ .

Figure 2(d) shows the  $I_{\text{dc}}$ -induced shift  $\Delta H_{\text{FMR}}$  as a function of the in-plane magnetization angle, equal to the applied field angle  $\theta$  for the soft NiFe layer. This angular dependence is well described by a  $\sin \theta$  relation, which implies that  $H_I$  is transverse to the current axis. Figure 2(e) shows that the constant  $H_I = -\Delta H_{\text{FMR}}/\sin \theta$  indeed agrees well with the PHE data measured at  $\theta \approx 0$ . This finding confirms that  $H_I$ , including the non-Oersted contribution, is

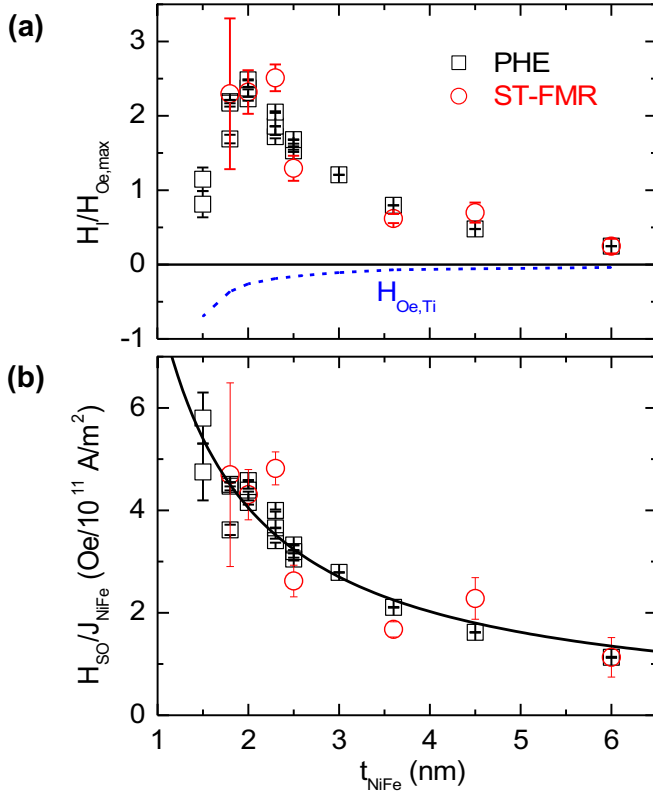


FIG. 3. (a) NiFe thickness  $t_{NiFe}$  dependence of  $H_1$  normalized by  $H_{Oe,max}$ . The dotted curve indicates the estimated Oersted field from Ti,  $H_{Oe,Ti}$ . Each ST-FMR data point is the mean of results at several frequencies 3.5–7.0 GHz at  $\theta = 45^\circ$  and  $-135^\circ$ .  $H_1/H_{Oe,max} > 0$  is defined as  $H_1 \parallel +y$  when  $I_{dc} \parallel +x$  [illustrated in Figs. 1(a) and 2(a)]. (b) Estimated spin-orbit field  $H_{SO}$  per unit current density in NiFe,  $J_{NiFe}$ . The solid curve indicates the fit to  $t_{NiFe}^{-1}$ .

entirely transverse to the current and is independent of the magnetization orientation.

In Fig. 3(a), we plot the dependence of  $H_1$  (normalized by  $H_{Oe,max}$  for clarity) on NiFe thickness  $t_{NiFe}$ . The two independent techniques, PHE at low applied fields and ST-FMR at high applied fields [34], confirm the presence of  $H_1$  that cannot be accounted for by the Oersted field alone for a wide range of  $t_{NiFe}$ . The observed  $H_1$  opposes  $H_{Oe,Ti}$  in all samples, and  $H_1$  is more than a factor of 2 larger than  $H_{Oe,max}$  at  $t_{NiFe} \approx 2$  nm. The drop in  $H_1$  for  $t_{NiFe} \lesssim 2$  nm is caused by the increasing magnitude of  $H_{Oe,Ti}$ , as NiFe becomes more resistive and a larger fraction of current flows through Ti with decreasing  $t_{NiFe}$ .

The anomalous portion of  $H_1$ , which cannot be explained by the classical Oersted field, may be due to a spin-orbit torque that acts as a “spin-orbit field”  $H_{SO}$ . In Fig. 3(b), we plot the estimated  $H_{SO} = H_1 - H_{Oe,Ti}$  normalized by the current density in NiFe,  $J_{NiFe}$ . This normalized  $H_{SO}$  scales inversely with  $t_{NiFe}$ , implying that the source of  $H_{SO}$  is outside or at a surface of the NiFe layer. Therefore,  $H_{SO}$  does not arise from spin-orbit effects within the bulk of NiFe [35], i.e., the reciprocal of the recently reported inverse spin Hall effect in FMs [36–39]. Moreover, any possible spin-orbit torques arising from the bulk of NiFe would depend on the

magnetization orientation [35] and are thus incompatible with the observed symmetry of  $H_{SO}$  [Fig. 2(e)]. It is unlikely that  $H_{SO}$  is generated by the spin Hall effect in Ti, because its spin Hall angle is small ( $<0.001$ ) [40,41] and only a small fraction of  $I_{dc}$  is expected to be in the resistive ultrathin Ti layer. In Ti/NiFe/Al<sub>2</sub>O<sub>3</sub>, we also do not observe a dampinglike torque that would be expected to arise from the spin Hall effect [6,42]; the linewidth  $W$  is invariant with  $I_{dc}$  within our experimental resolution  $\lesssim 0.2$  Oe/mA [33].

With spin-orbit effects in the bulk of NiFe and Ti ruled out as mechanisms behind  $H_{SO}$ , the only known mechanism that agrees with the observed  $H_{SO}$  is the Rashba-Edelstein effect [1,4,5], with an interfacial spin accumulation (polarized transverse to the current) exchange coupling to the magnetization in NiFe. Indeed, tight-binding Rashba model calculations reveal a fieldlike torque, but no dampinglike torque, in the first order of spin-orbit coupling due to transverse spin accumulation that is independent of the magnetization orientation [43].

We now gain further insight into the origin of  $H_{SO}$  by examining its dependence on the layer stack structure, as summarized in Figs. 4(a)–4(f). In the symmetric Al<sub>2</sub>O<sub>3</sub>(1.5 nm)/NiFe(2.3 nm)/Al<sub>2</sub>O<sub>3</sub>(1.5 nm) trilayer [Fig. 4(a)],  $H_1$  vanishes, which is as expected because the Oersted field should be nearly zero and the two nominally identical interfaces sandwiching NiFe produce no net spin accumulation. Breaking structural inversion symmetry with the Ti(1.2 nm) seed layer results in an uncompensated interfacial spin accumulation that generates a finite  $H_{SO} = H_1 - H_{Oe,Ti}$  [Fig. 4(b)].

Inserting Pt(0.5 nm) between the NiFe and Al<sub>2</sub>O<sub>3</sub> layers suppresses  $H_{SO}$ , such that the estimated Oersted field  $H_{Oe,NM}$  from the nonmagnetic Ti and Pt layers entirely accounts for  $H_1$  [Fig. 4(c)]. This may seem counterintuitive since Pt exhibits strong spin-orbit coupling and a large Rashba-Edelstein effect may be expected [44]. However, Pt is also a strong spin scatterer, as evidenced by an increase in the Gilbert damping parameter from  $\approx 0.013$  for Ti/NiFe/Al<sub>2</sub>O<sub>3</sub> to  $\approx 0.03$  for Ti/NiFe/Pt/Al<sub>2</sub>O<sub>3</sub>. Any accumulated spins may quickly become scattered by Pt, such that there is no net fieldlike torque mediated by exchange coupling [4,5] between these spins and the magnetization in NiFe [45]. Based on the suppression of  $H_{SO}$  by Pt insertion, we infer that the Rashba-Edelstein effect at the NiFe/Al<sub>2</sub>O<sub>3</sub> interface is the source of  $H_{SO}$ .

We observe another unexpected result upon inserting a layer of Cu, a metal with nearly zero bulk spin-orbit coupling, at the NiFe/Al<sub>2</sub>O<sub>3</sub> interface: The direction of  $H_{SO} = H_1 - H_{Oe,NM}$  is reversed [Fig. 4(d)]. Just as in Ti/NiFe/Al<sub>2</sub>O<sub>3</sub>, this observed  $H_{SO}$  in Ti/NiFe/Cu/Al<sub>2</sub>O<sub>3</sub> is independent of magnetization orientation, and no dampinglike torque is detected within our experimental resolution. We deduce a Rashba-Edelstein effect (opposite in sign to that of NiFe/Al<sub>2</sub>O<sub>3</sub>) at the Cu/Al<sub>2</sub>O<sub>3</sub> interface, rather than the NiFe/Cu interface, because (1) if NiFe/Cu generates the reversed  $H_{SO}$ , we should see an enhanced  $H_{SO}$  for NiFe sandwiched between Cu (bottom) and Al<sub>2</sub>O<sub>3</sub> (top), but this is not the case [Fig. 4(e)], and (2) inserting a spin-scattering layer of Pt(0.5 nm) between Cu and Al<sub>2</sub>O<sub>3</sub> suppresses  $H_{SO}$  [Fig. 4(f)]. Figure 4(g) plots the dependence of  $H_1$  on Cu thickness  $t_{Cu}$ . In the limit of large  $t_{Cu}$  ( $\approx 10$  nm),  $H_1$  approaches  $H_{Oe,NM}$  that is predominantly due to the current in the highly conductive Cu layer. From the estimated current

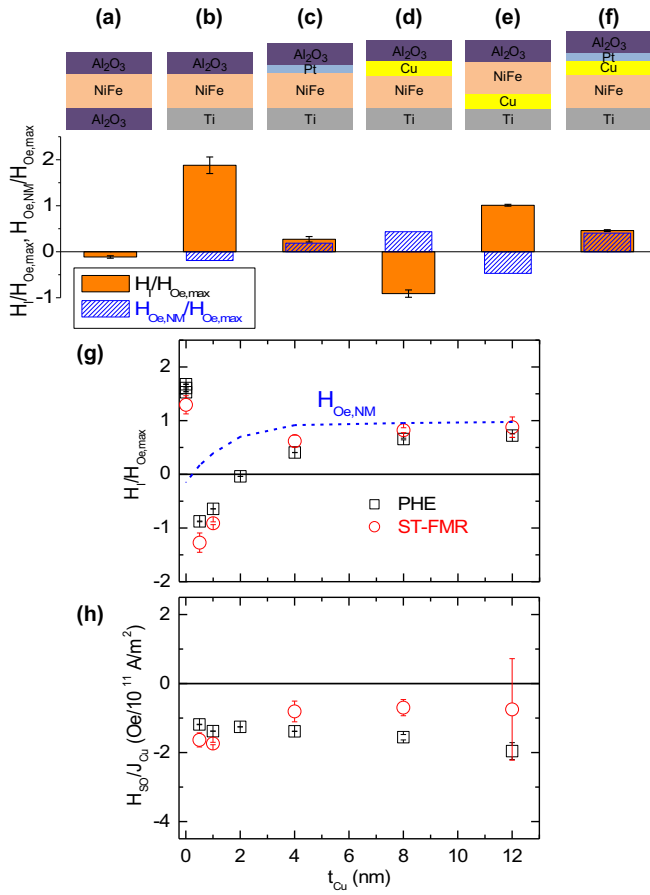


FIG. 4. (a)–(f) Structural dependence of  $H_I$  (mean of measurements on three PHE devices) normalized by  $H_{Oe,max}$ .  $H_{Oe,NM}$  is the Oersted field from current in the nonmagnetic metal layers (Ti, Cu, Pt). The nominal layer thicknesses are as follows: NiFe, 2.3 nm; Al<sub>2</sub>O<sub>3</sub>, 1.5 nm; Ti, 1.2 nm; Cu, 1.0 nm; and Pt, 0.5 nm. (g) Cu thickness  $t_{Cu}$  dependence of  $H_I$  normalized by  $H_{Oe,max}$  at NiFe thickness 2.5 nm. The blue dotted curve indicates  $H_{Oe,NM}$ . (h) Estimated spin-orbit field  $H_{SO}$  per unit current density in Cu,  $J_{Cu}$ .

distribution, we obtain  $H_{SO} = H_I - H_{Oe,NM}$  normalized by the current density in the Cu layer,  $J_{Cu}$ . As shown in Fig. 4(h),  $H_{SO}/J_{Cu} \approx -1-2$  Oe/10<sup>11</sup> A/m<sup>2</sup> exhibits little dependence on  $t_{Cu}$ . This is consistent with the Rashba-Edelstein effect at the Cu/Al<sub>2</sub>O<sub>3</sub> interface that is present irrespective of  $t_{Cu}$ .

Persistence of  $H_{SO}$  even at large  $t_{Cu}$  indicates a nonlocal Rashba-Edelstein field, whereas the absence of a dampinglike torque implies negligible diffusive (dissipative) spin transport from the Cu/Al<sub>2</sub>O<sub>3</sub> interface to the NiFe layer. Evidently, the spin accumulation at the Cu/Al<sub>2</sub>O<sub>3</sub> interface exchange couples to the magnetization in NiFe across the Cu layer. However, further studies are required to elucidate the mechanism involving Cu, since we do not observe any apparent oscillation

in  $H_{SO}$  with  $t_{Cu}$  that would be expected for exchange coupling across Cu [46]. Theoretical studies may also clarify why the directions of  $H_{SO}$  arising from NiFe/Al<sub>2</sub>O<sub>3</sub> and Cu/Al<sub>2</sub>O<sub>3</sub> are opposite. Another outstanding question that can be addressed by further experimental work is how the level of oxidation or disorder at the metal/insulator interface influences  $H_{SO}$ .

At  $t_{Cu} \approx 2$  nm,  $H_I$  vanishes because  $H_{SO}$  and  $H_{Oe,NM}$  compensate each other [Fig. 4(g)]. Fan *et al.* also show near vanishing of  $H_I$  in NiFe(2 nm)/Cu( $t_{Cu}$ )/SiO<sub>2</sub>(3.5 nm) at  $t_{Cu} \approx 3$  nm [10], and Avci *et al.* report a current-induced field in Co(2.5 nm)/Cu(6 nm)/AlO<sub>x</sub>(1 nm) that is well below the estimated Oersted field [20]. In each of these studies [10,20], a spin-orbit field due to the Rashba-Edelstein effect at the Cu/oxide interface may have counteracted the Oersted field. More generally, various metal/insulator interfaces, where the metal is ferromagnetic or nonmagnetic, may exhibit Rashba-Edelstein effects. In some HM/FM/oxide heterostructures, the Rashba-Edelstein torque from the FM/oxide interface may even dominate over torques from the HM bulk or HM/FM interface, e.g., when the HM is thin and hence resistive, which possibly explains the reported sign reversal in the fieldlike torque with decreasing HM thickness [13,19].

In summary, we have shown a current-induced spin-orbit torque due to Rashba-Edelstein effects at NiFe/Al<sub>2</sub>O<sub>3</sub> and Cu/Al<sub>2</sub>O<sub>3</sub> interfaces. This torque is distinct from previously reported spin-orbit torques in that it arises even without spin-orbit coupling in the bulk of the constituent materials. The origin of this torque is purely interfacial spin-orbit coupling, which likely emerges from the electric dipoles that develop at the metal/insulator interfaces [29,30]. This mechanism is supported by recent theoretical predictions of current-induced spin polarization at metal/insulator interfaces in the absence of bulk spin-orbit coupling [47–49]. Rashba-Edelstein effects at metal/insulator interfaces may be universal and should motivate the use of various previously neglected materials as components for enhancing spin-orbit torques and as model systems for interfacial spin-dependent physics, perhaps combined with gate-voltage tuning [21,22,50]. One possibility is to apply interfacial band alignment techniques, similar to those for semiconductor heterostructures [51], to control dipole-induced Rashba-Edelstein effects.

This work was supported by the AFRL through Contract No. FA8650-14-C-5706, the W. M. Keck Foundation, and the NSF TANMS ERC Award No. 1160504. X-ray reflectivity was performed in CMSE at MIT, and lithography was performed in the George J. Kostas Nanoscale Technology and Manufacturing Research Center. We thank Geoffrey Beach, Carl Boone, Xin Fan, Adrian Feiguin, Chi-Feng Pai, and Kohei Ueda for helpful discussions. We give special thanks to Mairbek Chshiev, Sergey Nikolaev, and Noriyuki Sato for their comments and sharing of unpublished results.

- [1] V. Edelstein, *Solid State Commun.* **73**, 233 (1990).
- [2] A. Hoffmann, *IEEE Trans. Magn.* **49**, 5172 (2013).
- [3] J. Sinova, S. O. Valenzuela, J. Wunderlich, C. H. Back, and T. Jungwirth, *Rev. Mod. Phys.* **87**, 1213 (2015).

- [4] A. Manchon and S. Zhang, *Phys. Rev. B* **78**, 212405 (2008).
- [5] P. Gambardella and I. M. Miron, *Philos. Trans. R. Soc., A* **369**, 3175 (2011).

- [6] P. M. Haney, H.-W. Lee, K.-J. Lee, A. Manchon, and M. D. Stiles, *Phys. Rev. B* **87**, 174411 (2013).
- [7] A. Brataas and K. M. D. Hals, *Nat. Nanotechnol.* **9**, 86 (2014).
- [8] A. Chernyshov, M. Overby, X. Liu, J. K. Furdyna, Y. Lyanda-Geller, and L. P. Rokhinson, *Nat. Phys.* **5**, 656 (2009).
- [9] L. Liu, O. J. Lee, T. J. Gudmundsen, D. C. Ralph, and R. A. Buhrman, *Phys. Rev. Lett.* **109**, 096602 (2012).
- [10] X. Fan, J. Wu, Y. Chen, M. J. Jerry, H. Zhang, and J. Q. Xiao, *Nat. Commun.* **4**, 1799 (2013).
- [11] X. Fan, H. Celik, J. Wu, C. Ni, K.-J. Lee, V. O. Lorenz, and J. Q. Xiao, *Nat. Commun.* **5**, 3042 (2014).
- [12] C.-F. Pai, M.-H. Nguyen, C. Belvin, L. H. Vilela-Leão, D. C. Ralph, and R. A. Buhrman, *Appl. Phys. Lett.* **104**, 082407 (2014).
- [13] M.-H. Nguyen, D. C. Ralph, and R. A. Buhrman, *Phys. Rev. Lett.* **116**, 126601 (2016).
- [14] I. M. Miron, K. Garello, G. Gaudin, P.-J. Zermatten, M. V. Costache, S. Auffret, S. Bandiera, B. Rodmacq, A. Schuhl, and P. Gambardella, *Nature (London)* **476**, 189 (2011).
- [15] T. D. Skinner, M. Wang, A. T. Hindmarch, A. W. Rushforth, A. C. Irvine, D. Heiss, H. Kurebayashi, and A. J. Ferguson, *Appl. Phys. Lett.* **104**, 062401 (2014).
- [16] M. Kawaguchi, T. Moriyama, T. Koyama, D. Chiba, and T. Ono, *J. Appl. Phys.* **117**, 17C730 (2015).
- [17] G. Allen, S. Manipatruni, D. E. Nikonov, M. Doczy, and I. A. Young, *Phys. Rev. B* **91**, 144412 (2015).
- [18] K. Garello, I. M. Miron, C. O. Avci, F. Freimuth, Y. Mokrousov, S. Blügel, S. Auffret, O. Boulle, G. Gaudin, and P. Gambardella, *Nat. Nanotechnol.* **8**, 587 (2013).
- [19] J. Kim, J. Sinha, M. Hayashi, M. Yamanouchi, S. Fukami, T. Suzuki, S. Mitani, and H. Ohno, *Nat. Mater.* **12**, 240 (2013).
- [20] C. O. Avci, K. Garello, M. Gabureac, A. Ghosh, A. Fuhrer, S. F. Alvarado, and P. Gambardella, *Phys. Rev. B* **90**, 224427 (2014).
- [21] R. H. Liu, W. L. Lim, and S. Urazhdin, *Phys. Rev. B* **89**, 220409 (2014).
- [22] S. Emori, U. Bauer, S. Woo, and G. S. D. Beach, *Appl. Phys. Lett.* **105**, 222401 (2014).
- [23] X. Qiu, K. Narayanapillai, Y. Wu, P. Deorani, D.-H. Yang, W.-S. Noh, J.-H. Park, K.-J. Lee, H.-W. Lee, and H. Yang, *Nat. Nanotechnol.* **10**, 333 (2015).
- [24] M. Akyol, G. Yu, J. G. Alzate, P. Upadhyaya, X. Li, K. L. Wong, A. Ekicibil, P. Khalili Amiri, and K. L. Wang, *Appl. Phys. Lett.* **106**, 162409 (2015).
- [25] N. Sato, A. El-Ghazaly, R. White, and S. Wang, *IEEE Trans. Magn.* (2016), doi:10.1109/TMAG.2016.2515025.
- [26] J. C. Rojas Sánchez, L. Vila, G. Desfonds, S. Gambarelli, J. P. Attané, J. M. De Teresa, C. Magén, and A. Fert, *Nat. Commun.* **4**, 2944 (2013).
- [27] K. Chen and S. Zhang, *Phys. Rev. Lett.* **114**, 126602 (2015).
- [28] W. Zhang, M. B. Jungfleisch, W. Jiang, Y. Liu, J. E. Pearson, S. G. E. te Velthuis, A. Hoffmann, F. Freimuth, and Y. Mokrousov, *Phys. Rev. B* **91**, 115316 (2015).
- [29] L. Xu and S. Zhang, *J. Appl. Phys.* **111**, 07C501 (2012).
- [30] F. Ibrahim, H. X. Yang, A. Hallal, B. Dieny, and M. Chshiev, *Phys. Rev. B* **93**, 014429 (2016).
- [31] L. Liu, T. Moriyama, D. C. Ralph, and R. A. Buhrman, *Phys. Rev. Lett.* **106**, 036601 (2011).
- [32] D. Fang, H. Kurebayashi, J. Wunderlich, K. Výborný, L. P. Zárbo, R. P. Campion, A. Casiraghi, B. L. Gallagher, T. Jungwirth, and A. J. Ferguson, *Nat. Nanotechnol.* **6**, 413 (2011).
- [33] T. Nan, S. Emori, C. T. Boone, X. Wang, T. M. Oxholm, J. G. Jones, B. M. Howe, G. J. Brown, and N. X. Sun, *Phys. Rev. B* **91**, 214416 (2015).
- [34] ST-FMR is conducted with maximum  $H = 800$  Oe. No dependence of  $H_I$  on  $H$  (or excitation frequency) was observed.
- [35] T. Taniguchi, J. Grollier, and M. D. Stiles, *Phys. Rev. Appl.* **3**, 044001 (2015).
- [36] B. F. Miao, S. Y. Huang, D. Qu, and C. L. Chien, *Phys. Rev. Lett.* **111**, 066602 (2013).
- [37] A. Tsukahara, Y. Ando, Y. Kitamura, H. Emoto, E. Shikoh, M. P. Delmo, T. Shinjo, and M. Shiraiishi, *Phys. Rev. B* **89**, 235317 (2014).
- [38] A. Azevedo, O. Alves Santos, R. O. Cunha, R. Rodríguez-Suárez, and S. M. Rezende, *Appl. Phys. Lett.* **104**, 152408 (2014).
- [39] H. Wang, C. Du, P. Chris Hammel, and F. Yang, *Appl. Phys. Lett.* **104**, 202405 (2014).
- [40] C. Du, H. Wang, F. Yang, and P. C. Hammel, *Phys. Rev. B* **90**, 140407 (2014).
- [41] K. Uchida, M. Ishida, T. Kikkawa, A. Kirihara, T. Murakami, and E. Saitoh, *J. Phys.: Condens. Matter* **26**, 343202 (2014).
- [42] F. Freimuth, S. Blügel, and Y. Mokrousov, *Phys. Rev. B* **90**, 174423 (2014).
- [43] A. Kalitsov, S. A. Nikolaev, J. Velev, W. H. Butler, M. Chshiev, and O. Mryasov, [arXiv:1604.07885](https://arxiv.org/abs/1604.07885).
- [44] H. J. Zhang, S. Yamamoto, Y. Fukaya, M. Maekawa, H. Li, A. Kawasuso, T. Seki, E. Saitoh, and K. Takanashi, *Sci. Rep.* **4**, 4844 (2014).
- [45] With the insertion of Pt(0.5 nm), while the fieldlike torque is suppressed, a small dampinglike torque emerges with an estimated effective spin Hall angle  $\theta_{DL}$  (defined in Ref. [33]) of  $\approx 0.01$ .
- [46] S. S. P. Parkin, *Phys. Rev. Lett.* **67**, 3598 (1991).
- [47] X. Wang, J. Xiao, A. Manchon, and S. Maekawa, *Phys. Rev. B* **87**, 081407 (2013).
- [48] J. Borge, C. Gorini, G. Vignale, and R. Raimondi, *Phys. Rev. B* **89**, 245443 (2014).
- [49] S. S.-L. Zhang, G. Vignale, and S. Zhang, *Phys. Rev. B* **92**, 024412 (2015).
- [50] U. Bauer, L. Yao, A. J. Tan, P. Agrawal, S. Emori, H. L. Tuller, S. van Dijken, and G. S. D. Beach, *Nat. Mater.* **14**, 174 (2015).
- [51] H. Kroemer, *Rev. Mod. Phys.* **73**, 783 (2001).